Global Variations of Zonal Mean Ozone during Stratospheric Warming Events

WILLIAM J. RANDEL

National Center for Atmospheric Research, Boulder, Colorado*

(Manuscript received 21 September 1992, in final form 25 March 1993)

ABSTRACT

Eight years of Solar Backscatter Ultraviolet ozone data are examined to study zonal mean ozone variations associated with stratospheric planetary wave (warming) events. These fluctuations are found to be nearly global in extent, with relatively large variations in the tropics, and coherent signatures reaching up to 50° in the opposite (summer) hemisphere. These ozone variations are a manifestation of the global circulation cells associated with stratospheric warming events; the ozone responds dynamically in the lower stratosphere to transport, and photochemically in the upper stratosphere to the circulation-induced temperature changes. The observed ozone variations in the tropics are of particular interest because transport is dominated by zonal-mean vertical motions (eddy flux divergences and mean meridional transports are negligible), and hence, substantial simplifications to the governing equations occur. The response of the atmosphere to these impulsive circulation changes provides a situation for robust estimates of the ozone–temperature sensitivity in the upper stratosphere.

1. Introduction

Monitoring of the global ozone distribution from satellites has provided the opportunity to assess variability over a wide range of space and time scales. Substantial efforts have gone into analyzing long time series of ozone for trends (WMO 1991; Stolarski et al. 1991) and also for quantifying seasonal and interannual variations (Bowman and Krueger 1985; Perliski and London 1989; Sun and Leovy 1990; Shiotani 1992). Satellite ozone data have also been useful for studying phenomena with shorter time scales, such as traveling synoptic-scale waves (Schoeberl and Krueger 1983) and breaking planetary waves (Leovy et al. 1985).

In this work we use eight years of Solar Backscatter Ultraviolet (SBUV) measurements to document variations of zonal mean ozone associated with planetary wave events in the winter hemisphere stratosphere (stratospheric warming events). These are the dominant fluctuations in zonal mean ozone on subseasonal time scales, and have the intriguing aspect of being near global in character. The variations documented here provide further evidence of coherent, global-scale circulation cells induced by episodic planetary wave events localized in the winter hemisphere stratosphere, as documented previously in stratospheric temperature measurements (Fritz and Soules 1972). Chandra (1986) and Sun and Leovy (1990) have also shown evidence from ozone observations for these short-term circulation variations. We extend those analyses by calculating the circulations directly, based on analyses of wind and temperature data derived from National Meteorological Center (NMC) stratospheric analyses. Due to different mapping procedures used on the ozone versus NMC data, it is necessary to smooth the NMC data in time to be directly comparable to the ozone data (details are found in the Appendix). We find strong coherence between direct measures of winter hemisphere wave activity and zonal mean temperature, wind, and ozone variations over the globe. The ozone mixing ratio perturbations exhibit a quadrupole pattern in the meridional plane between 25 and 50 km, with horizontal out-of-phase variations between the tropics and high winter latitudes, and vertical out-of-phase behavior between the lower and upper stratosphere; column ozone variations mirror those for mixing ratio in the lower stratosphere. The net effect of each wave event is a loss of total ozone in the tropics and increase over high winter latitudes (net transport towards the pole). Similar global ozone variations are found for wave events during Southern Hemisphere (SH) winter–spring, although the correlation patterns are somewhat weaker than those for the NH winter events.

The observed ozone fluctuations in the tropics are of particular interest here because transport is dominated by mean vertical advection (meridional advection and the direct effects of wave flux divergences are small). We directly compare observed ozone variations with those calculated from the zonal mean continuity equation, and find good quantitative agreement in the lower stratosphere (where transport is dominant). In

* The National Center for Atmospheric Research is sponsored by the National Science Foundation.

Corresponding author address: Dr. William J. Randel, NCAR, P.O. Box 3000, Boulder, CO 80307-3000.

the upper stratosphere, the photochemical production and loss terms are both an order of magnitude larger than observed tendencies, and small errors in their evaluation precludes accurate estimates of the observed tendencies. However, the strong coupling between the production and loss terms allows these data to be useful for robust estimates of the ozone–temperature sensitivity in the tropics, which may in turn be compared with results from photochemical models. Observational estimates made here give results in the upper stratosphere that are somewhat higher than ratios resulting from a recent model calculation. Furthermore, the observations show a meridional maximum in the ozone–temperature sensitivity over the equator, whereas the model calculation positions the maximum in the summer subtropics.

This study of zonal mean ozone variability complements previous studies of balances in the eddy (zonally asymmetric) components. Overall agreement between calculated and observed variations have been found using SBUV and NMC data for local balances during NH winter (Douglass et al. 1985), and for fluctuations attributable to global-scale traveling planetary waves (Randel 1993). Both of these studies, together with Douglass and Rood (1986) and Froidevaux et al. (1989), compare observed ozone–temperature sensitivities with linear parameterization estimates, for variations due to middle-latitude eddies. The zonal mean analyses here focus on the tropics and hence complement those studies. Furthermore, observations of zonal mean fluctuations are less sensitive to the uncertainties associated with local (latitude–longitude) variability.

2. Data and analyses

The ozone data analyzed here are daily vertical profile and column amounts obtained from the SBUV instrument, which flew on the *Nimbus-7* spacecraft from late 1978 to early 1987. The ozone trends panel report (WMO 1991) discusses the information content of SBUV data, concluding that it should be capable of resolving the ozone profile from 16 to 0.5 mb (approximately 28 to 56 km), with a vertical resolution near 8–10 km. The data used here are mixing ratios at pressure levels 30, 20, 10, 7, 5, 3, 2, 1, 0.5, and 0.3 mb, which is oversampled in the vertical, along with the column ozone amount. The profile and column data were horizontally mapped using a Kalman filter, giving an estimate of the zonal mean (and zonal waves 1–6) on a 4-degree latitude grid. Missing days' data (approximately one in four days prior to mid-1983) are interpolated by the Kalman algorithm. Because of missing data during polar night, ozone data only up to 64° latitude are analyzed for the respective winter hemispheres. For the purpose of estimating the vertical gradient of ozone at the lowest level (30 mb), the SBUV zonal mean data were extended down to 50 mb using time-averaged zonal mean ozone data from LIMS (Gille and Russell 1984).

Temperature and wind data used here are derived from daily operational stratospheric geopotential height analyses at 70, 50, 30, 10, 5, 2, and 1 mb produced at the National Meteorological Center/Climate Analysis Center (NMC/CAC). These data are derived mainly from satellite measurements with similar space–time sampling as that for the SBUV data. The NMC analyses are, however, mapped horizontally using a successive correction (Cressman) analysis scheme. As shown in the Appendix, this Cressman mapping scheme results in more high-frequency variability for zonal mean data than that found for the same data mapped with the Kalman scheme. This difference is important if quantitative comparisons between these data are to be made. In order to make these two datasets more compatible, a low-pass digital filter was designed to approximate the observed Kalman to Cressman frequency response ratio (see Appendix; the filter's frequency response is shown in Fig. A3). This smoothing filter was applied to all time series derived from the NMC data prior to further analyses.

The zonal mean continuity equation for ozone mixing ratio written in the transformed Eulerian mean (TEM) formalism is

$$\frac{\partial \bar{\mu}}{\partial t} + \overline{v^*}\bar{\mu}_y + \overline{w^*}\bar{\mu}_z = \bar{S} + \frac{1}{\rho_0}\nabla \cdot \mathbf{M} \qquad (1)$$

[Eq. (9.4.13) of Andrews et al. 1987]. Here $\bar{\mu}$ is the zonal-mean mixing ratio, $\overline{v^*}$ and $\overline{w^*}$ components of the mean meridional circulation, $\bar{S}$ a source/sink term, and $(1/\rho_0)\nabla \cdot \mathbf{M}$ is an eddy transport term. Equation (1) suggests that *tendencies* of zonal mean ozone ($\partial\bar{\mu}/\partial t$) rather than ozone mixing ratio itself will be most strongly correlated with variations of the large scale circulation ($\overline{v^*}$, $\overline{w^*}$), and we focus attention here on calculated ozone tendencies. Analysis of ozone tendencies also has the advantage of effectively removing slow variations due to background seasonality. One further advantage is that the long-term drifts in SBUV ozone (Fleig et al. 1986) and changes in NMC-derived temperatures due to satellite changes (Gelman et al. 1986) are effectively removed by examining time tendencies.

Cross-correlations are used in this paper to deliniate the spatial structure of coherent variations in the meridional plane. Correlations are calculated from time series of length 120 days, centered on NH winter (December–February) and SH winter–spring (August–October), and averaged over the eight years of data covering late 1978–1986. Significance levels are estimated from Eq. (A8) of Lau and Chan (1983), using a conservative estimate of 10 days for the autocorrelation *e*-folding time for the variables here. Correlations of size 0.22 and 0.28 correspond to confidence levels of 95% and 99%, respectively.

Statistical estimates of the ozone–temperature ratio $(\bar{\mu} - \bar{\mu}_0)/(\bar{T} - \bar{T}_0)$ in section 3c are made using empirical orthogonal function (EOF) analyses of the respective time series. Standard regression analysis (of one time series upon the other) assumes no measurement error in the regressor time series, and minimizes the squared residuals with respect to that time series. In the case here, where both ozone and temperature time series possess measurement uncertainties, an EOF analysis is a more robust method to estimate the slopes (the EOF scheme minimizes residuals in a direction normal to the derived slope estimate). A simple expression for the EOF-derived slope (a_1) is given by

$$a_1 = \tan\left[\frac{1}{2}\tan^{-1}\left(\frac{2 \cdot \mathrm{SXY}}{\mathrm{SXX} - \mathrm{SYY}}\right)\right]. \qquad (2)$$

Here $\mathrm{SXY} = \Sigma(\bar{\mu} - \bar{\mu}_0)(\bar{T} - \bar{T}_0)$, $\mathrm{SXX} = \Sigma(\bar{T} - \bar{T}_0)^2$, and $\mathrm{SYY} = \Sigma(\bar{\mu} - \bar{\mu}_0)^2$, with sums over the available observations. Standard regression analysis also has the undesirable property that the derived regression coefficient is proportional to the correlation coefficient, so that regression estimates are biased low for weaker correlated time series. Tests on synthetic time series with varying added noise levels show that the EOF technique gives more robust estimates of the slope for cases where the overall time series correlation decreases. Uncertainty estimates for the slope (2) are calculated using the standard formulas in chapter 8.4 of Chatfield (1978).

3. Results

a. *Patterns of zonal mean variability*

Figure 1 shows the latitude–time evolution of the zonal mean ozone at 2 mb over 1979–1981. A similar seasonal evolution is seen for each year, with largest mixing ratios observed in high latitudes of the winter hemisphere, and small values in summer. Superimposed on this seasonal cycle are large perturbations associated with midwinter stratospheric warming events; these are clear in the NH during January 1980 and 1981 and in the SH during July 1979 and August 1981. (Interestingly, the 2-mb zonal mean ozone patterns seen in Fig. 1 look qualitatively similar to the zonal wind evolution in the upper stratosphere, with ozone maxima more or less overlying the polar night jet, and midwinter warmings being evidenced by strong sudden decreases in both variables.) The structure of the ozone perturbations at 2 mb during the warming events is such that ozone decreases at high winter latitudes, and increase in low latitudes. Time series of these data at 52°N and at the equator are shown in Fig. 2, together with the zonal mean tendencies at these latitudes. Note that the calculated tendencies highlight the shorter period variations associated with midwinter wave events, and that the tendencies are mostly out of phase between high and low latitudes during the northern winters (equatorial variations during SH winters are out of phase with high Southern Hemisphere latitudes). There is a distinct semiannual variation in the equatorial ozone time series in Fig. 2, with the associated ozone maxima clearly related in time to wave events in the respective winter hemispheres [previously analyzed and discussed in Dunkerton and Delisi (1988) and Sun and Leovy (1990)].

Figure 3a shows a meridional cross section of the daily standard deviation of $\partial\bar{\mu}/\partial t$ calculated over December–February, averaged over the eight years of data. Two regions of maximum variance are observed: one in the high-latitude winter upper stratosphere, and one centered over the equator in the middle-upper stratosphere. Although temperature variations during stratospheric warmings are much larger in high latitudes than in the tropics (see Fig. 5), ozone fluctuations are more similarly sized between high and low latitudes, because ozone is much more sensitive to temperature

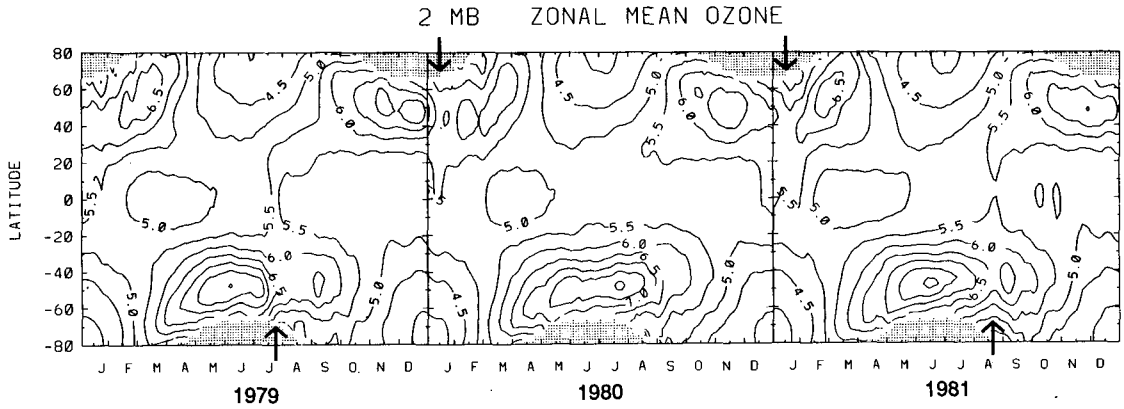

FIG. 1. Latitude–time section of zonal mean ozone at 2 mb, covering the years 1979–1981. Contour interval is 0.5 ppmv. Polar night regions where no SBUV data are available are noted by shading. Arrows denote large amplitude winter hemisphere wave events.

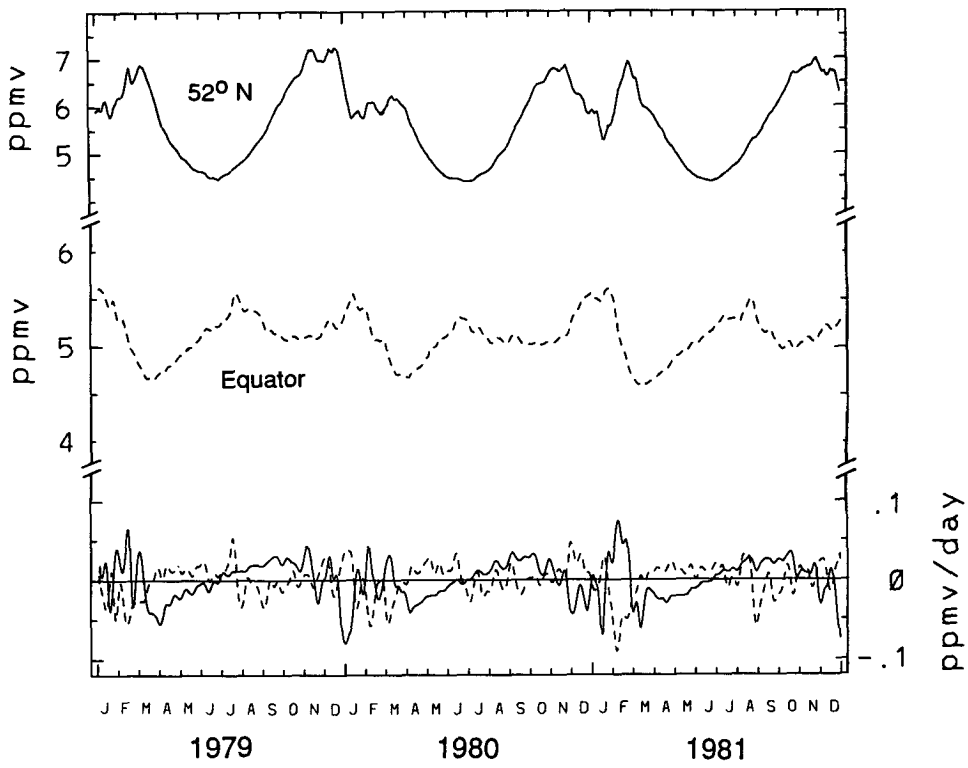

FIG. 2. The top two curves are time series of 2-mb zonal mean ozone at 52°N and the equator, from SBUV data over 1979–1981 (as in Fig. 1). The curves at the bottom are the time tendencies calculated from the respective time series, with the dashed line values multiplied by two for clarity.

in the tropics. The predominant pattern of spatial variability for ozone tendency is shown via a one-point correlation map in the meridional plane (Fig. 3b), using a base point at 52°N, 2 mb. The high latitude and tropical tendency maxima in the upper stratosphere show strong out-of-phase behavior (as seen in the time series for the 2-mb level in Fig. 2). Additionally, there is a region of strong correlation in the lower stratosphere over the tropics, in phase with the reference position (and out of phase with variations in the tropical upper stratosphere). Note that these low-latitude correlations extend well into the summer hemisphere, and that the overall patterns are truly global in nature.

b. *Coherence with stratospheric planetary wave events*

The global variations in zonal mean ozone highlighted in Figs. 1–3 are clearly related to winter stratospheric warming events, driven by episodic planetary wave activity. In order to quantify this relationship, this section demonstrates that strong cross correlations exist between the ozone variations and direct measures of the high-latitude winter wave activity itself. For the latter, we choose time series of the eddy heat flux $\overline{v'T'}$ at 60°N, 50 mb. This choice of reference time series for wave activity is made mainly because this quantity signals the episodic vertical propagation of wave activity from the troposphere into the stratosphere, and is strongly correlated with all other measures of wave activity (e.g., Randel et al. 1987). Other reference time series for planetary wave activity (such as kinetic energy or EP flux divergence) and other reference positions were tested, and all give results qualitatively the same as those shown here.

Figure 4 shows an example of the reference heat flux time series during the NH winter 1979/80 (cf. Figs. 1–2). There are six distinct wave events during this winter, the last five of which hint at a periodicity of 2–3 weeks. Some other NH winters show similar periodicity, while for other NH winters and most SH winters the episodes appear more randomly. Madden (1975, 1983) has discussed this 2–3-week periodicity in the NH winter stratosphere, suggesting an explanation via the interference of stationary and traveling planetary waves. In any case, the main point here is to demonstrate correlations between the planetary wave events (whatever their cause) and zonal mean ozone variability. Included in Fig. 4 are time series of zonal mean ozone and temperature tendencies over 0°–30°S, for the 30-mb and 2-mb pressure levels. These latter time series show fluctuations that are clearly correlated in time with the $\overline{v'T'}$ time series variations. Note that

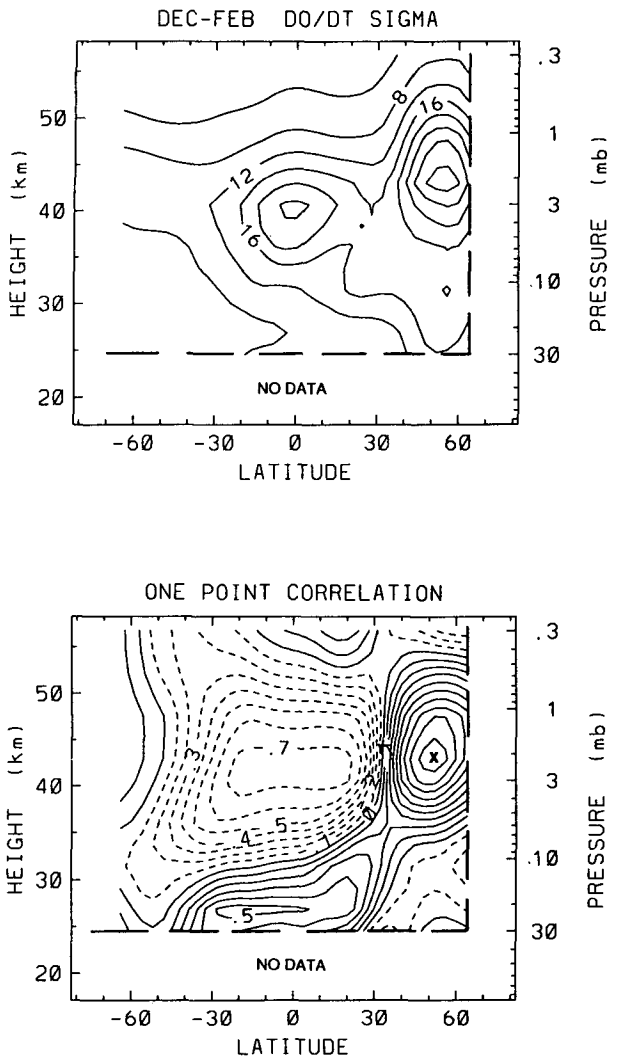

FIG. 3. (top) Meridional cross section of daily standard deviation of zonal mean ozone tendency $\partial\bar{\mu}/\partial t$, with units of 10^{-3} ppmv/day. (bottom) One-point correlation map of zonal mean ozone tendency, with respect to a reference position at 52°N, 2 mb. Both panels were calculated from eight years of NH winter data.

the ozone and temperature tendencies are in phase at 30 mb and out of phase at 2 mb in Fig. 4.

The global patterns of ozone and temperature changes associated with one particular wave event are shown in Fig. 5. These maps were constructed from differences calculated over 1–14 January 1980, corresponding to the second wave event seen in Fig. 4. Stratospheric temperature changes show an increase of order 10–20 K throughout winter high latitudes, and cooling of order 2–3 K over the tropics and into the SH (up to 50°S). Such global temperature variations were originally documented in satellite data by Fritz and Soules (1972). The ozone changes for this event (presented as local percentage differences in Fig. 5b) show maxima of order 10%–15% in the upper stratosphere (out of phase with the temperature changes), and differences of order 4% in the lower stratosphere (in phase with temperature).

Figure 6 shows the column ozone over 0°–30°S during the 1979/80 winter period. Superimposed on the seasonal downward trend are variations of several Dobson units associated with the winter wave activity variations. This relationship is clarified by examining the *tendency* of column ozone (middle curve in Fig. 6): episodes of strong column decrease in the tropics are clearly correlated with enhanced winter hemisphere planetary wave amplitudes. In fact, time periods when the wave activity becomes small (i.e., the middle of December, the middle of January, and early February in Fig. 6) correspond to near-zero tendency of column ozone in the tropics. This association suggests that winter hemisphere stratospheric wave activity is linked, via the induced mean circulations, to the downward *seasonal* trend of total ozone in the summer subtropics during November–March and July–October (see Bowman and Krueger 1985, their Fig. 9). This seasonal time-scale circulation effect in the summer subtropics can also be seen in the N_2O and CH_4 data analyzed by Holton and Choi (1988) (see their Figs. 1–2); these tracers both show the effects of upwelling centered near

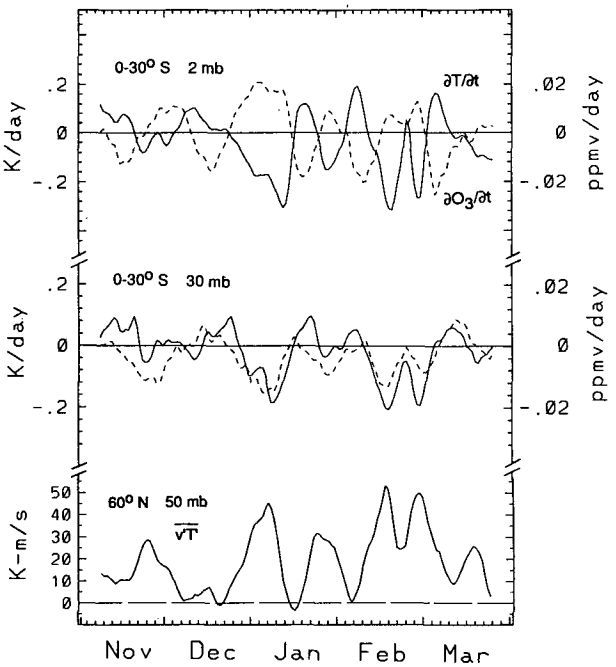

FIG. 4. Time series of selected variables during the NH winter of 1979/80. The bottom curve is the poleward heat flux ($\overline{v'T'}$) at 60°N, 50 mb, used as a reference time series for planetary wave variations in the stratosphere. The other curves show observed zonal mean ozone (dashed) and temperature (solid) tendencies over 0°–30°S, at 30 mb (middle) and at 2 mb (top). Note the correlations between NH winter wave events and zonal mean tendencies in the summer subtropics, and the in- and out-of-phase behavior of ozone and temperature tendencies at 30 and 2 mb.

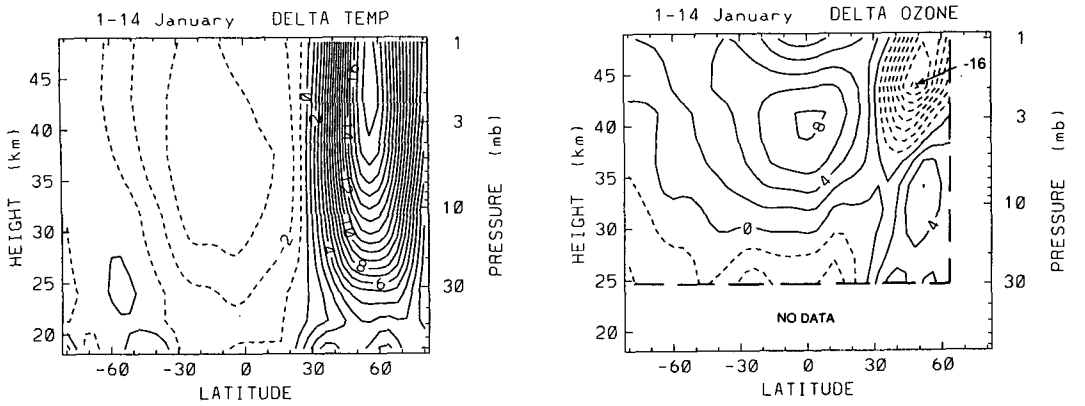

FIG. 5. Meridional cross sections of zonal mean temperature (left) and ozone (right) changes over 1–14 January 1980, accompanying a NH winter planetary wave event. Ozone differences are calculated as percentages with respect to the zonal mean values on 1 January.

20° in the summer hemisphere, maximizing during periods of wave activity in the winter stratosphere.

The correlation between the ozone tendency at each latitude and height and the reference $\overline{v'T'}$ time series (at 60°N, 50 mb) is shown as a contour map in Fig. 7; these correlations are averaged over the eight years of NH winter data. Added in the lower panel in Fig. 7 are the correlations with the column ozone tendency. Also shown in Fig. 7 is a map of the correlations with zonal mean temperature tendency; these diagrams are the statistical equivalents of the single event patterns shown in Fig. 5. Positive correlations in these diagrams indicate local increases of ozone or temperature coincident with the planetary wave events. Strong ozone tendency correlations are found throughout the meridional plane in Fig. 7, with structure similar to the one-point correlation map in Fig. 3b and the individual event pattern in Fig. 5b; this conclusively demonstrates that the ozone oscillations identified in Figs. 1–2 are due to planetary wave events. The ozone patterns in Fig. 7 show an overall quadrupole pattern of tendencies associated with the planetary waves, with out-of-phase variations on either side of 40°N and between the lower and upper stratosphere. The column tendencies mirror the mixing ratio patterns in the lower stratosphere, showing ozone decrease over 40°S–30°N, and increase polewards of 50°N. The quadrupole pattern of ozone variability over 25–50 km is a robust result, also observed for wave events in idealized model results (Rose and Brasseur 1989, their Fig. 5). Temperature tendencies in Fig. 7 show heating throughout the stratosphere polewards of 40°N, and cooling extending throughout the tropics up to 60°S. Comparison of the temperature and ozone tendency correlations in Fig. 7 shows that they are in phase in the lower stratosphere and out of phase in the upper stratosphere.

These observed patterns of zonal mean temperature changes (Figs. 5a and 7a) are in good agreement with those calculated for idealized planetary wave forcings in the winter stratosphere. Figure 8 shows global temperature changes forced by localized NH stratosphere wave driving, oscillating with a period of 15 days, calculated by Garcia (1987). Note the good agreement between the calculation in Fig. 8 and the observations

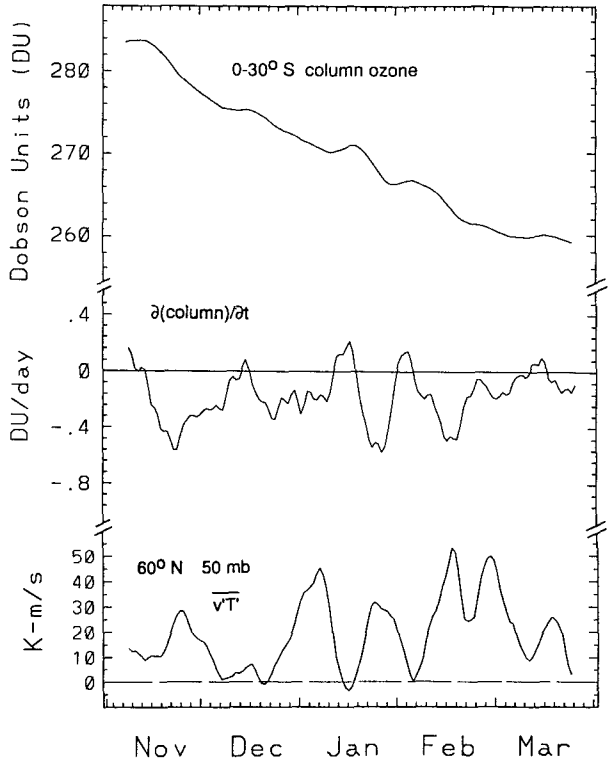

FIG. 6. The top curve shows the total column ozone over 0°–30°S during NH winter 1979/1980, and the middle curve is the calculated tendency. Bottom curve is the reference heat flux time series in the North Polar stratosphere (identical to that in Fig. 4). Note that the periods of strongest column ozone decrease are correlated with wave events.

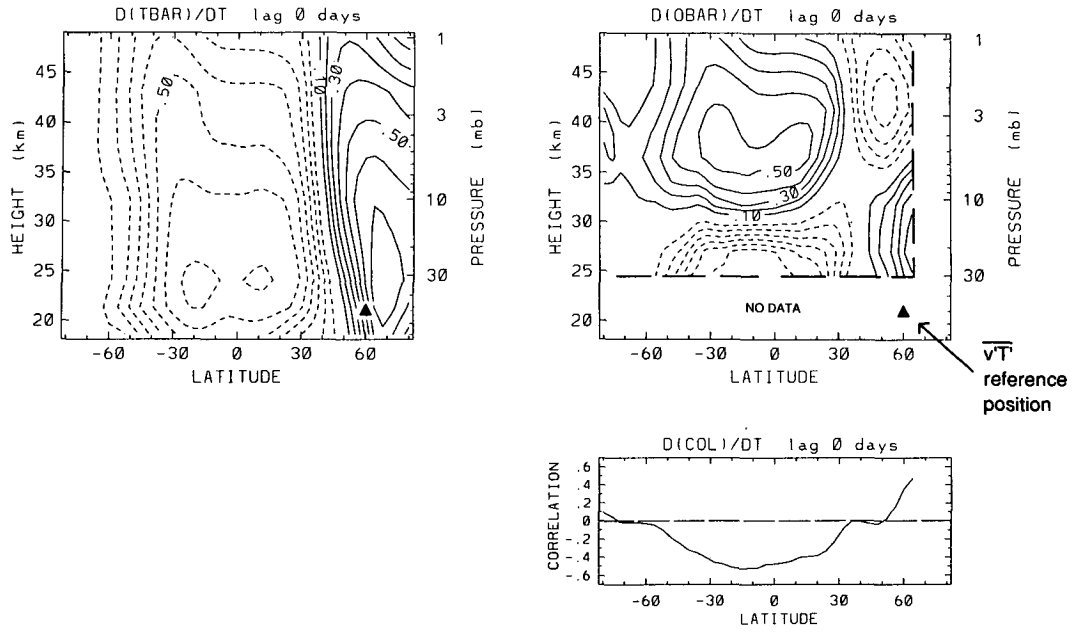

FIG. 7. Meridional cross section of correlations between zonal mean temperature (left) and ozone (right) tendencies at each latitude and height with the reference heat flux time series at 60°N, 50 mb. These results are averages over eight years of NH winter data. Contour interval is 0.1, with zero contours omitted. Because of lack of polar night data, ozone correlations are not calculated polewards of 64°N. The bottom curve on the right shows the correlations with the total column ozone tendency.

in Figs. 5a–7a (the latter being a statistical pattern), most notably for variations in the tropics and in the SH (far from the direct wave forcing). Such agreement highlights the robust character of the forced meridional circulation cells. As a note, the calculations shown in Fig. 8 extend to 80 km, and there are temperature changes over 45–80 km that are out of phase with those over 10–45 km. These mesospheric temperature changes are not analyzed in our results in Fig. 5a–7a (which extend only to ~50 km), but are observed in other studies (Labitzke 1972; Gille et al. 1983).

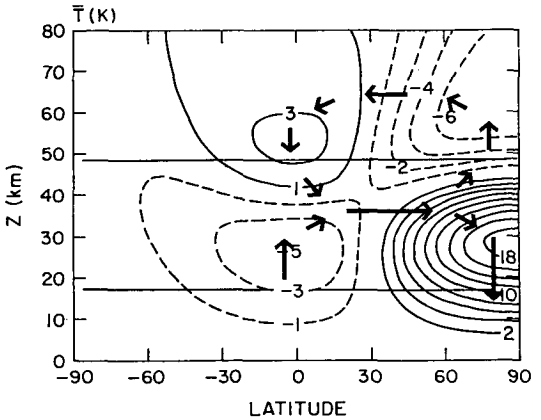

FIG. 8. Calculated zonal mean temperature response to episodic wave driving imposed in the NH stratosphere, taken from the model results of Garcia (1987). Also shown schematically are components of the wave-driven residual circulation ($\bar{v}^*$, $\bar{w}^*$). Note the good agreement between observations (Fig. 5a) and these calculations over the region 20–50 km (noted by the horizontal lines).

Figure 9 shows ozone and temperature tendency correlations calculated for data during SH winter–spring (August–October), using $\overline{v'T'}$ reference time series at 50 mb, 60°S. Note that the ozone data extend to the winter pole during this period. The patterns in Fig. 9 are qualitatively similar to those in Fig. 7, but with somewhat reduced correlations in both quantities in the upper stratosphere (above 5 mb), and also weaker meridional extent into the summer hemisphere. These weaker correlations suggest that the residual circulations forced by planetary waves during SH winter are weaker than those during NH winter, likely due to weaker wave forcing during SH winter, and to the more intense zonal winds and larger inertial stability of the SH polar vortex. The column tendency in Fig. 9 shows that wave events decrease column ozone over the tropics and increase it in high winter latitudes, in agreement with the NH winter data.

c. *Quantitative estimates of ozone change in the tropics*

The coherent ozone variations found in the tropics during planetary wave events invite further analyses. The reason that this region is of special interest is that simplifying assumptions can be applied to Eq. (1). Mean meridional advection $\bar{v}^* \bar{\mu}_y$ can be neglected in

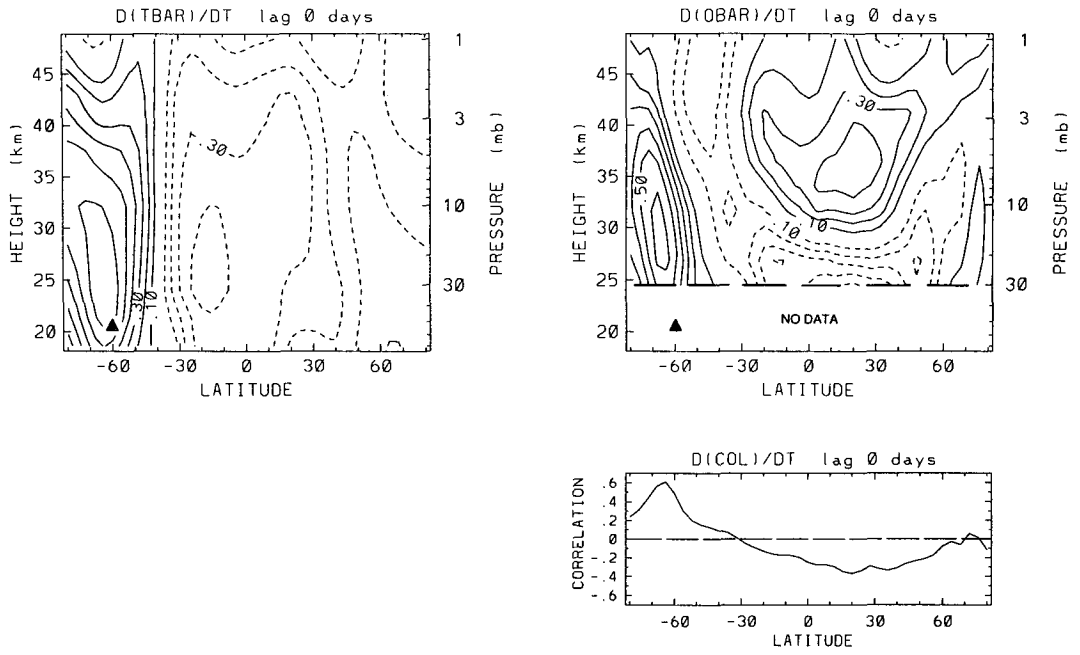

FIG. 9. Southern Hemisphere winter–spring correlations between zonal mean temperature (left) and ozone (right) tendencies, with respect to a reference time series of heat flux at 60°S, 50 mb. Contour interval is 0.1, with zero contours omitted. The panel at lower right shows the corresponding correlation with the column ozone tendency.

the tropics because $\bar{\mu}_y$ is small; this was confirmed using the residual circulation calculated by Garcia (1987), as shown in Fig. 8, and realistic ozone gradients. Furthermore, the tropics are far removed from the direct effects of wave transience in the winter stratosphere [the $(1/\rho_0)\nabla\cdot\mathbf{M}$ term in Eq. (1)]. Hence, Eq. (1) simplifies to

$$\frac{\partial\bar{\mu}}{\partial t} + \overline{w^*}\bar{\mu}_z = \bar{S}. \tag{3a}$$

One common approximation for the photochemical source/sink term $\bar{S}$ is to use terms that are linear in ozone and temperature deviations from some specified background state (Hartmann and Garcia 1979; Douglass et al. 1985). Such a linearization applied to zonal mean perturbations takes the form

$$\bar{S} = -\Gamma(\bar{\mu} - \bar{\mu}_0) - \theta(\bar{T} - \bar{T}_0), \tag{3b}$$

where Γ and θ are photochemical parameters (taken here from the calculations of Stolarski and Douglass 1985), and $\bar{\mu}_0$ and $\bar{T}_0$ are temporarily smoothed "background" zonal mean values. The background values are calculated here using a running Gaussian-shaped smoother, with a width of approximately one month. Estimates of $\overline{w^*}$ are obtained from the zonal mean thermodynamic equation, again neglecting the meridional advection term in the tropics:

$$\frac{\partial\bar{T}}{\partial t} + \overline{w^*}\frac{H}{R}N^2 = -\alpha(\bar{T} - \bar{T}_0). \tag{4}$$

The expression on the right-hand side represents a Newtonian damping term, with α an inverse damping time scale taken from Gille and Lyjak (1986, Fig. 13), and $\bar{T}_0$ calculated as above.

Figure 10 shows rms values of each term in Eq. (3) versus pressure in the tropics during NH winter, with $\partial\bar{\mu}/\partial t$ calculated from observations. Figure 10 also shows the correlation between observed $\partial\bar{\mu}/\partial t$ and that calculated from Eq. (3). The observed and calculated values of $\partial\bar{\mu}/\partial t$ are correlated at the 30- and 5-mb levels, but not at 10, 2, and 1 mb. By inspection of the rms values of individual terms in Fig. 10, we separate the following analyses between the transport controlled region (30 mb), where $\overline{w^*}\bar{\mu}_z \gg \Gamma(\bar{\mu} - \bar{\mu}_0)$, and the photochemically controlled region (5, 2, and 1 mb), where $\Gamma(\bar{\mu} - \bar{\mu}_0) \gg \overline{w^*}\bar{\mu}_z$. Note the relative smallness of the $\overline{w^*}\bar{\mu}_z$ term at 5 mb in Fig. 10, showing that transport has relatively little effect at and above this level.

1) TRANSPORT REGION (30 MB)

Figure 11 shows time series of observed $\partial\bar{\mu}/\partial t$ during NH winter 1979/80, at 30 mb and averaged over 4°–12°S, together with the value calculated from Eq. (3) (this latitude band is chosen to minimize $\bar{\mu}_y$). Overall there is very good agreement between the observed and calculated tendencies. At 30 mb the ozone source–sink term is negligible (see Fig. 10), as is the Newtonian

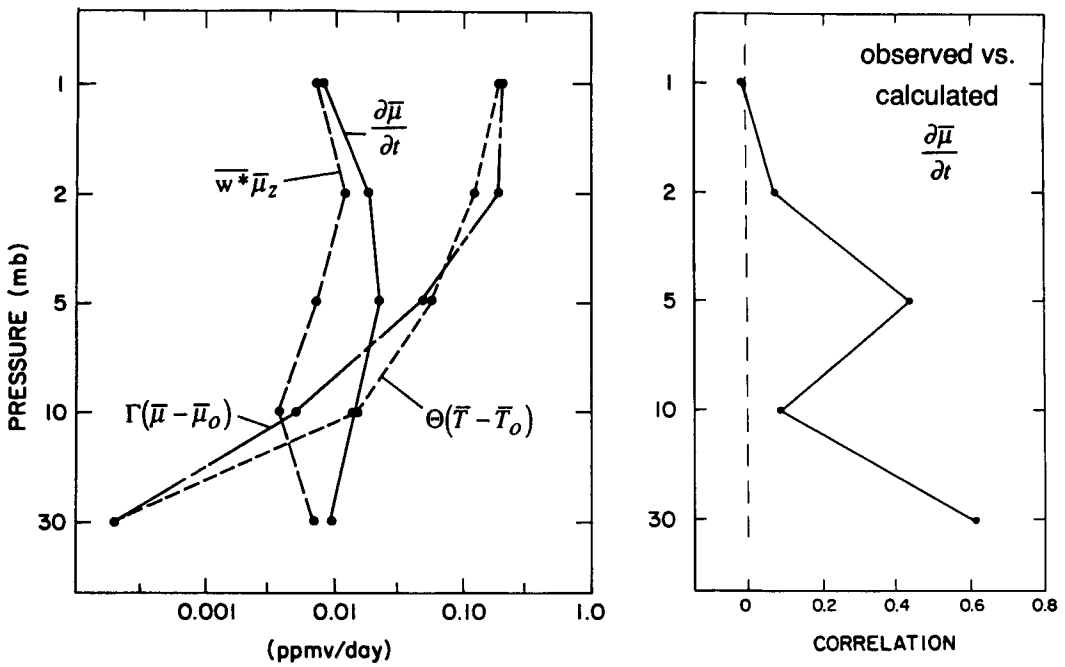

FIG. 10. (left) Vertical profile of rms values of terms in Eq. (3), evaluated over 4°–12°S, where tropical $\bar{\mu}_y$ terms are negligibly small. Note the logarithmic horizontal axis. (right) Correlation between observed ozone tendency ($\partial\bar{\mu}/\partial t$) and that calculated by Eq. (3), also over 4°–12°S. Both calculations use data averaged over eight NH winters.

damping term in Eq. (4). Equations (3)–(4) then combine to give

$$\frac{\partial\bar{\mu}}{\partial t} = \frac{\partial\bar{T}}{\partial t}\left(\frac{R}{H}\frac{\bar{\mu}_z}{N^2}\right). \tag{5}$$

This linear relationship is clearly seen in Fig. 4. The ratio of $\partial\bar{\mu}/\partial t$ to $\partial\bar{T}/\partial t$ at 30 mb over 4°–12°S, calculated via (2) from all eight years of data, gives a value of 0.055 ± 0.018 (ppmv/K), using two sigma uncertainties. Using tropical 30-mb background values of $\bar{\mu}_z \approx 0.7$ ppmv/km and $N^2 \sim 4.6 \times 10^{-4}$ s^{-2}, Eq. (5) gives an estimated ratio of 0.062 ppmv K^{-1}, in basic agreement with the values calculated from these observations.

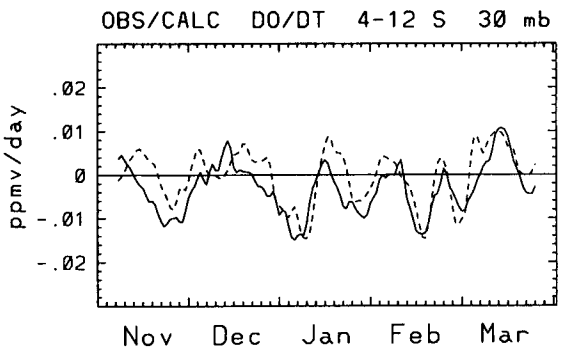

FIG. 11. Time series of observed (solid) and calculated (dashed) zonal mean ozone tendency at 30 mb over 4°–12°S, for data during NH winter 1979/1980. The calculated values [from Eq. (3)] are due entirely to the vertical transport term.

2) PHOTOCHEMICAL REGION (5, 2, AND 1 MB)

The fundamental balance for Eq. (2) in the upper stratosphere is $\Gamma(\bar{\mu} - \bar{\mu}_0) = -\theta(\bar{T} - \bar{T}_0)$; $\partial\bar{\mu}/\partial t$ and $\overline{w^*}\bar{\mu}_z$ are both an order of magnitude smaller than these terms at 2 and 1 mb, and more than a factor of 2 smaller at 5 mb (Fig. 10). The lack of correlation between calculated and observed $\partial\bar{\mu}/\partial t$ at 2 and 1 mb (Fig. 10) is simply due to the fact that small errors in either photochemical term overwhelm any signal attributable to $\partial\bar{\mu}/\partial t$. However, this strong coupling between the $\Gamma(\bar{\mu} - \bar{\mu}_0)$ and $\theta(\bar{T} - \bar{T}_0)$ terms at these levels is useful for comparing observed and parameterized ozone–temperature sensitivity in the upper stratosphere. In particular, this balance may be written

$$\frac{(\bar{\mu} - \bar{\mu}_0)}{(\bar{T} - \bar{T}_0)} = -\frac{\theta}{\Gamma},$$

and the observed ratio $(\bar{\mu} - \bar{\mu}_0)/(\bar{T} - \bar{T}_0)$ can be compared to $-\theta/\Gamma$. The large signals afforded by the episodic wave events, in particular the isolated signals in the tropics, provide a most robust observational test of the parameter values.

Figure 12 shows observed ozone ($\bar{\mu}$) and temperature ($\bar{T}$) at 2 mb and 8°S during NH winter 1979/80,

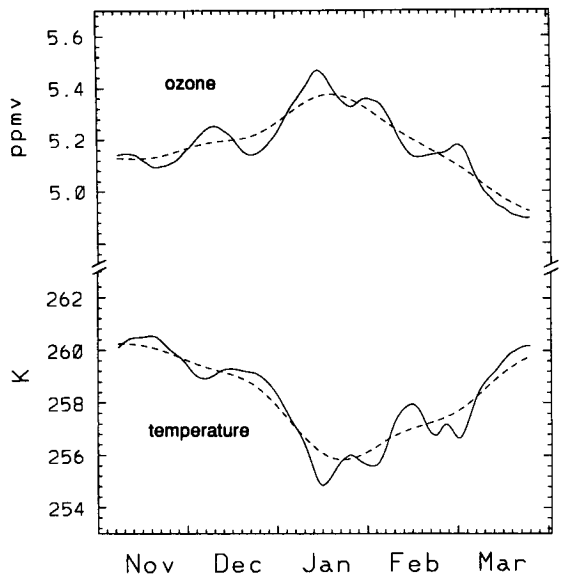

FIG. 12. Solid lines are observed variations of zonal mean ozone (top) and temperature (bottom) at 8°S, 2 mb, during NH winter 1979/80. The dashed lines are smoothed versions of these curves, used for estimates of the "background" values. The differences between the actual and smoothed curves are the $(\bar{\mu} - \bar{\mu}_0)$ and $(\bar{T} - \bar{T}_0)$ values used in Eq. (3b).

along with smoothed "background" values $(\bar{\mu}_0)$ and $(\bar{T}_0)$. The deviations $(\bar{\mu} - \bar{\mu}_0)$ and $(\bar{T} - \bar{T}_0)$ in Fig. 12 are strongly anticorrelated: Fig. 13 shows cross sections of the correlation between these variables averaged over the eight years of NH winter and SH winter data. Figure 13 shows very similar results for both seasons: strong negative correlations are observed throughout the upper stratosphere, with maxima over the tropics and polar winter latitudes. Strong positive correlations are found in the lower stratosphere. The line of zero correlation is approximately 5–10 km lower in the tropics than in high latitudes of either summer or winter hemisphere.

The ratio $(\bar{\mu} - \bar{\mu}_0)/(\bar{T} - \bar{T}_0)$ is obtained from these data by the EOF analysis (2) discussed in section 2. Figure 14 shows a scatterplot of $(\bar{\mu} - \bar{\mu}_0)$ versus $(\bar{T} - \bar{T}_0)$ at 2 mb, 8°S, using all eight NH winters of data. The data in Fig. 14 are strongly correlated ($r = -0.89$), and give a slope of -0.074 ± 0.009 ppmv K^{-1}. This derived slope, along with those at 5 and 1 mb, are compared to the θ/Γ ratios from Stolarski and Douglass (1985) in Fig. 15 (all using data averaged over 0°–16°S). The ozone–temperature slope derived from these data is approximately 50% larger than the parameterized value at 2 mb. The observed and calculated values at 1 mb are in good agreement, while the estimated slope at 5 mb is approximately 15% smaller than their calculation (although the two sigma error bars do barely overlap their value). Figure 16 shows the meridional structure of the derived and parameterized values at 2 mb. In addition to the observations being somewhat larger than the parameterized values, the observations have a maximum over the equator, while the parameterized values show a broad maximum over 0°–20°S. The observed maximum $(\bar{\mu} - \bar{\mu}_0)/(\bar{T} - \bar{T}_0)$ ratio situated symmetrically over the equator is also seen in the ozone tendency variance map in Fig. 3a and the ozone difference pattern in Fig. 5b; note that a similar map for temperature changes (Fig. 5a) does not show a maximum at the equator, but a broad maximum over 0°–20°S. Overall, there are significant differences between the ozone–temperature sensitivities derived from these data versus the parameterized values. These differences are discussed below.

4. Discussion

The tropical temperature changes that accompany stratospheric warming events (Fritz and Soules 1972) are remarkable evidence of the global-scale response

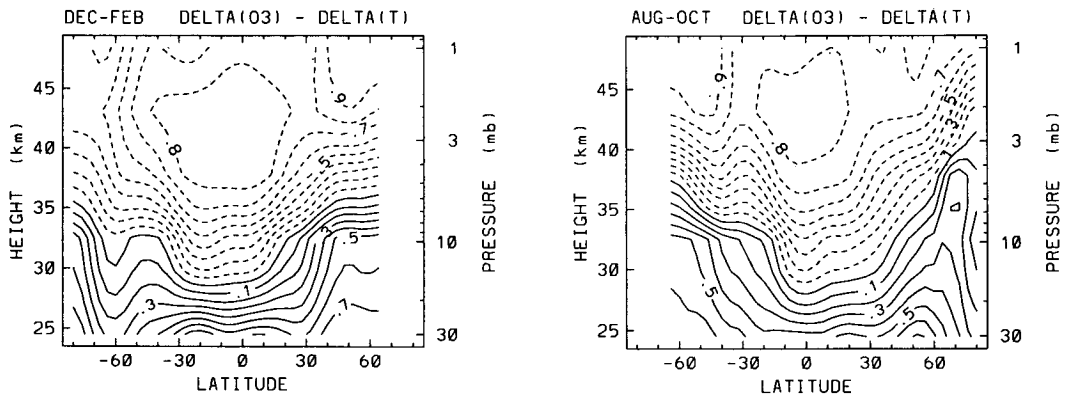

FIG. 13. Meridional cross sections of the correlation between $(\bar{\mu} - \bar{\mu}_0)$ and $(\bar{T} - \bar{T}_0)$ time series (see Fig. 12), averaged over the eight years of data during NH winter (left) and SH winter–spring (right).

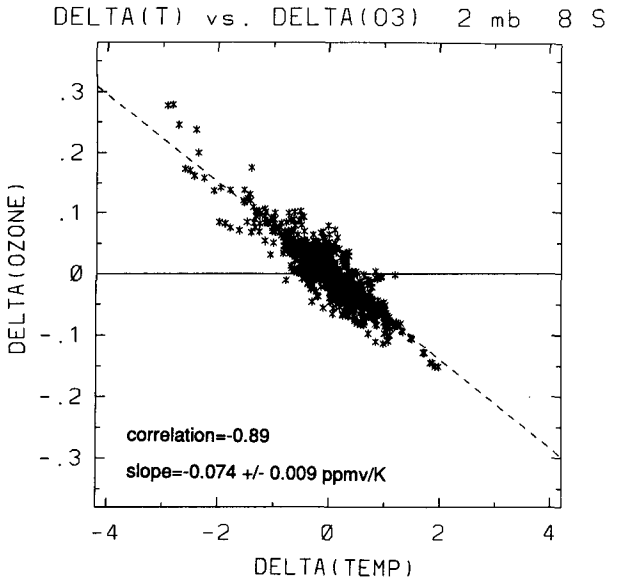

FIG. 14. Scatter diagram of $(\bar{\mu} - \bar{\mu}_0)$ versus $(\bar{T} - \bar{T}_0)$ at 8°S, 2 mb, for the eight years of NH winter data. The dashed line shows the slope fit by the EOF analysis discussed in section 2.

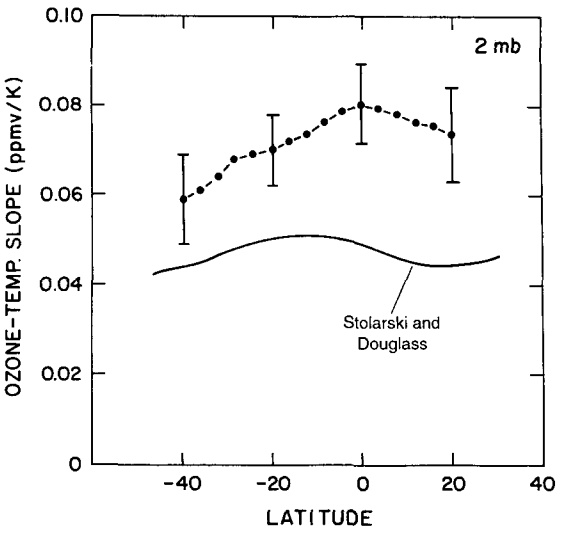

FIG. 16. Latitudinal variation of the ozone–temperature slope at 2 mb, calculated from the observations here, and that given by the parameter values of Stolarski and Douglass (1985) (solid line).

of the atmosphere to localized wave-driven forcing. The response of a geostrophically balanced vortex to such localized forcing, and the associated global meridional circulations, have been discussed theoretically by Eliassen (1951), Dunkerton et al. (1981), Plumb (1982), and Garcia (1987). Gille et al. (1987, their Fig. 6) have clearly shown that the mean vertical circulation exhibits strong episodic variability on these time scales, with global-scale coherence. Here we have shown further evidence of these global circulations in zonal mean ozone data. The episodic and coherent nature of mean meridional transport processes associated with planetary wave events is attractive for isolating their signatures from other variability. As opposed to the problem of integrated transport over monthly time scales (Solomon et al. 1986; Holton and Choi 1988; Stanford et al. 1993), analysis of individual wave events allows detailed study of individual terms in the constituent continuity equation.

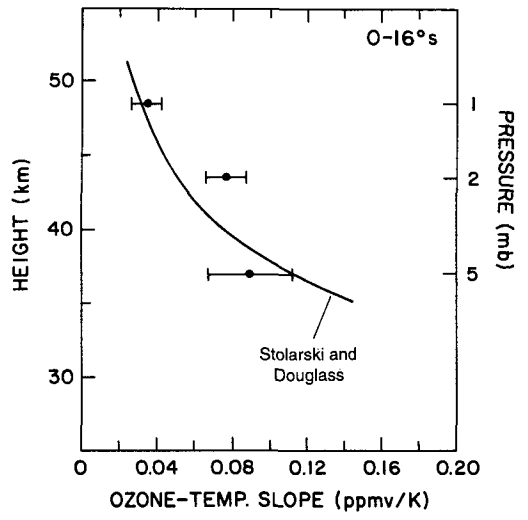

FIG. 15. Comparison of the ozone–temperature slopes at 5, 2, and 1 mb calculated from the data here, with the θ/Γ parameter values of Stolarski and Douglass (1985) (solid line), for NH winter data averaged over 0°–16°S. Error bars on the observations show a two standard deviation variance on either side of the central estimate.

Along these lines, analysis of forced variations in the tropics offer still further simplifications. The direct effect of the winter stratosphere eddies are negligible in the tropics, and for a constituent such as ozone, with small meridional gradients in the tropics, the mean meridional advection term may also be neglected. Hence vertical transport is the sole remaining term for dynamical variability. The accuracy of these approximations is confirmed here by the good agreement between observed tropical ozone tendencies at 30 mb and those calculated from vertical transport alone (Fig. 11).

Similar calculations of the ozone tendency in the photochemically controlled upper stratosphere show some correlation with observed values at 5 mb, but near-zero correlations at 2 and 1 mb. The reason for the poor agreement at upper levels is that the tendency term is an order of magnitude less than the photochemical source and sink terms. Although these latter terms primarily cancel, small errors in their evaluation lead to differences that are as large or larger than the actual tendencies. Thus, without exceedingly accurate

(to 1%) evaluations of these photochemical terms, it seems that accurate tendencies cannot be calculated.

The tight coupling of the photochemical terms in the upper stratosphere is very useful, however, for calculating observed ozone–temperature sensitivities in the tropics. The deviations of ozone and temperature from their respective background (seasonal) trends are highly correlated in the tropics (Fig. 13), leading naturally to regression estimates of the ozone–temperature slope. The observations here give estimated slopes nearly 50% larger than the parameter values of Stolarski and Douglass (1985) at 2 mb. Values at 1 mb are in good agreement with their calculations, while observed estimates at 5 mb are approximately 15% smaller than their values (although two sigma error limits do marginally overlap their numbers). One caveat to all these comparisons is that the vertical resolution of the satellite instruments involved here is no better than approximately 10 km, so that the ozone–temperature slopes estimated here (e.g., Fig. 15) actually apply to measurements over finite vertical layers. In spite of this, the observed slopes at 2 mb are so much larger than calculated values that it appears that the differences are significant. One possible explanation for the relatively large difference at 2 mb is that the Stolarski and Douglass parameterization scheme considers only perturbations at one particular height, whereas in reality the variations have vertical coherence over deep layers. The effect of similarly signed ozone changes above 2 mb would be a relative decrease in downwelling ultraviolet radiation and hence photolysis rates at 2 mb, leading to less ozone loss and hence larger net ozone–temperature sensitivity at 2 mb. Hartmann (1978) has analyzed this question in some detail, suggesting that a 50% variation in the relaxation rate of ozone perturbations can occur by neglect of the vertical structure; this is similar to the differences reported here.

A more perplexing question is how to reconcile the observed and calculated meridional profiles shown in Fig. 16. This difference is less prone to satellite sampling questions. The maximum in ozone–temperature sensitivity over the equator can be seen directly in Fig. 5: the ozone changes show a clear peak over the equator, whereas the temperature changes show a broad maximum over 0°–20°S, and hence the ozone–temperature ratio is peaked over the equator. This sensitivity explains the observed maximum in ozone variance over the equator in the upper stratosphere (Fig. 3a). At present we can offer no explanation for this difference between the observed and calculated ozone behavior.

Acknowledgments. The author thanks Anne Douglass for several discussions regarding interpretation of the results shown here, and Kevin Trenberth for discussions on the regression and EOF analyses. Constructive reviews and suggestions were provided by Rolando Garcia, Roland Madden, and Masato Shiotani. The Kalman mapping of the ozone data was implemented by John Gille, Dan Packman, and Paul Bailey. The manuscript was expertly prepared by Marilena Stone. This work was supported under NASA Grant W-16215.

APPENDIX

Kalman versus Cressman Mapping of Zonal Means

A direct comparison of Kalman versus Cressman mapping of satellite-derived stratospheric data is made here to quantify variability derived using the two schemes. The two datasets compared here use the same satellite-derived ozone measurements, covering September 1985–February 1986. The Kalman mapped data is that used throughout this paper, while the Cressman mapped data was obtained from separate daily analyses archived at NMC/CAC, generated using the same mapping scheme as that applied to the NMC geopotential height data (R. Nagatani 1991, personal communication).

The Kalman mapping analysis fits a smooth curve in time to all available observations within a given latitude range (±2°), producing an estimate of the zonal mean and zonal wave components. The degree to

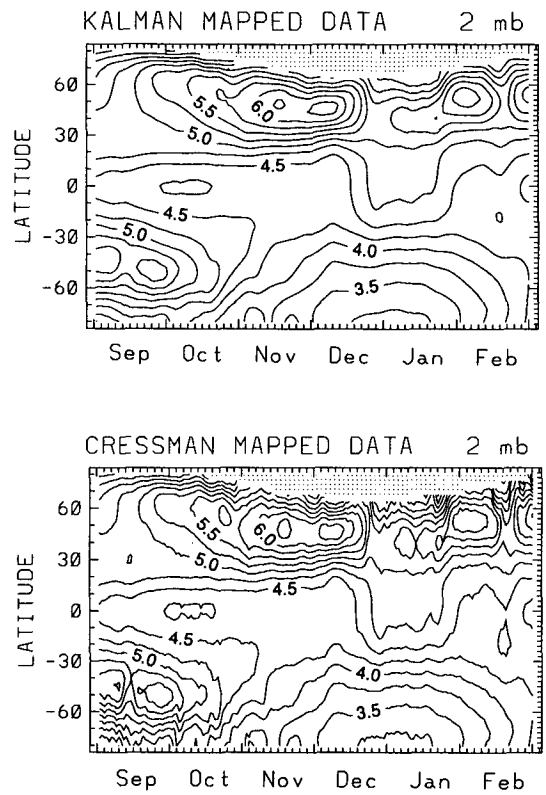

FIG. A1. Latitude–time sections of SBUV zonal mean ozone at 2 mb for data over September 1985–February 1986, mapped using the Kalman filter (top) and Cressman analysis (bottom).

which the observations are fit (and consequently the smoothness in space and time) is determined by the covariance of the data themselves, along with an estimate of the measurement noise. Time sampling may be done at any desired interval (once daily here). The Cressman mapping scheme is more local in both space and time. It uses all available observations within a specified horizontal radius (400 km) and within ±6 hours of the analysis time (once daily) to update a local gridpoint estimate (with the previous or first-guess value given by the prior day's analysis). We focus here on zonal means, and compare the longitudinally averaged Cressman data with the zonal means output directly by the Kalman analysis.

Figure A1 shows latitude–time evolution of the zonal mean ozone at 2 mb produced by the two mappings. Near-identical overall patterns are seen in the two plots, but the Kalman mapped data is notably smoother in time. This smoother time variation of the Kalman data is more pronounced when the time tendency is evaluated, as is the case for this work (the time tendency acts as a high-pass filter). Figure A2a shows time series of the zonal mean ozone tendency at 60°N calculated from the two mappings, clearly showing the 10–30-day fluctuations which are the subject of this paper.

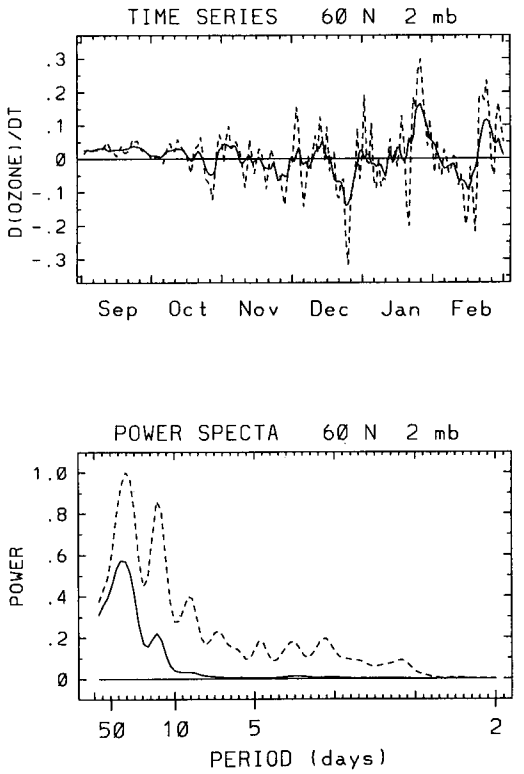

FIG. A2. (top) Time series of zonal mean ozone tendency ($\partial\bar{\mu}/\partial t$) at 60°N, 2 mb, calculated from the Kalman (solid) and Cressman (dashed lines) data. (bottom) Temporal power spectra calculated from the time series above. Units are arbitrary.

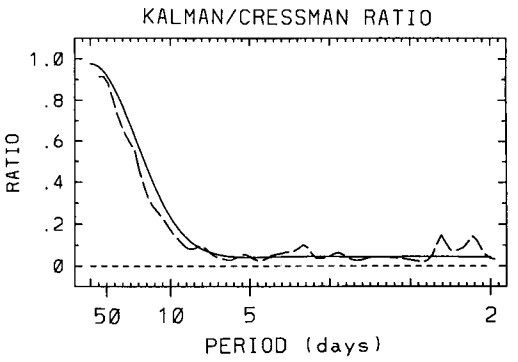

FIG. A3. Dashed line is the ratio of the spectral powers obtained from the Kalman and Cressman mapped data, that is, the ratio of the curves shown in Fig. A2b. Solid line is the squared amplitude response of the digital filter designed to smooth the Cressman data time series.

Although the same qualitative evolution is traced in both time series, the sizes of the peaks in the Cressman mapped data are nearly twice those from the Kalman data. Clearly this will have an adverse effect if quantitative comparisons between the two datasets are to be made (as between the Kalman mapped ozone and Cressman mapped temperature data here).

In order to alleviate this problem as much as possible, a digital filter is designed that can be used to smooth time series of Cressman mapped data to approximate the Kalman data. The desired frequency response of the digital filter is chosen based on comparing power spectra of the Kalman and Cressman data; Fig. A2b shows such power spectra calculated from the time series in Fig. A2a. Figure A3 shows the ratio of the two power spectra in Fig. A3; the power ratio is near 1.0 at lowest frequencies, falling off smoothly to small values at periods shorter than 10 days. Coefficients for the digital filter were calculated following Hamming (1989), and the squared amplitude response is included in Fig. A3. The resulting filtered Cressman time series shows good quantitative agreement with the Kalman data (not shown here).

The use of this smoothing filter on the NMC data affects the results presented here in two ways. First, the cross correlations between the NMC and Kalman mapped ozone data (Figs. 7, 9, and 13) are increased slightly (approximately 20%) using the filtered data; however, identical spatial patterns are obtained when unfiltered NMC data are used. Secondly, the ozone–temperature slopes calculated using unfiltered NMC data are 10%–20% smaller than those shown here, due to the inclusion of larger daily temperature deviations (for example, note the larger daily variations seen in Fig. A2). The large daily deviations seen in unfiltered NMC data are not a characteristic of Kalman mapped data, and the digital filter applied here is simply an attempt to put the two datasets on a common footing before quantitative comparisons are made.

REFERENCES

Andrews, D. G., J. R. Holton, and C. B. Leovy, 1987: *Middle Atmosphere Dynamics.* Academic Press, 489 pp.

Bowman, K. P., and A. J. Krueger, 1985: A global climatology of total ozone from the *Nimbus-7* total ozone mapping spectrometer. *J. Geophys. Res.*, **90,** 7967–7976.

Chandra, S., 1986: The solar and dynamically induced oscillations in the stratosphere. *J. Geophys. Res.*, **91,** 2719–2734.

Chatfield, C., 1978: *Statistics for Technology.* 2d ed. Chapman and Hall, 370 pp.

Douglass, A. R., R. B. Rood, and R. S. Stolarski, 1985: Interpretation of ozone–temperature correlations 2. Analysis of SBUV ozone data. *J. Geophys. Res.*, **90,** 10 693–10 708.

Dunkerton, T. J., and D. P. Delisi, 1988: Seasonal variation of the semiannual oscillation. *J. Atmos. Sci.*, **45,** 2772–2787.

——, C. P. F. Hsu, and M. E. McIntyre, 1981: Some Eulerian and Lagrangian diagnostics for a model stratospheric warming. *J. Atmos. Sci.*, **38,** 819–843.

Eliassen, A., 1951: Slow thermally or frictionally controlled circulation in a circular vortex. *Astrophys. Norv.*, **5**(2), 19–60.

Fleig, A. J., P. K. Bhartia, and D. S. Silberstein, 1986: An assessment of the long-term drift in SBUV total ozone data, based on comparison with the Dobson network. *Geophys. Res. Lett.*, **13,** 1359–1362.

Fritz, S., and D. Soules, 1972: Planetary variations of stratospheric temperature. *Mon. Wea. Rev.*, **100,** 582–589.

Froidevaux, L., M. Allen, S. Berman, and A. Daughton, 1989: The mean ozone profile and its temperature sensitivity in the upper stratosphere and lower mesosphere: An analysis of LIMS observations. *J. Geophys. Res.*, **94,** 6389–6417.

Garcia, R. R., 1987: On the mean meridional circulation of the middle atmosphere. *J. Atmos. Sci.*, **44,** 3599–3609.

Gelman, M. E., A. J. Miller, K. W. Johnson, and R. M. Nagatani, 1986: Detection of long-term trends in global stratospheric temperature from NMC analyses derived from NOAA satellite data. *Adv. Space Res.*, **6** (10), 17–26.

Gille, J. C., and J. M. Russell III, 1984: The Limb Infrared Monitor of the stratosphere: Experiment description, performance, and results. *J. Geophys. Res.*, **89,** 5125–5140.

——, and L. V. Lyjak, 1986: Radiative heating and cooling rates in the middle atmosphere. *J. Atmos. Sci.*, **43,** 2215–2229.

——, P. L. Bailey, L. V. Lyjak, and J. M. Russell III, 1983: Results from the LIMS experiment for the PMP-1 winter 1978/79. *Adv. Space Res.*, **2,** 163–167.

——, L. V. Lyjak, and A. K. Smith, 1987: The global residual mean circulation in the middle atmosphere for the Northern Winter period. *J. Atmos. Sci.*, **44,** 1437–1452.

Hamming, R. W., 1989: *Digital Filters.* 3d ed. Prentice-Hall, 284 pp.

Hartmann, D. L., 1978: A note concerning the effect of varying extinction on radiative-photochemical relaxation. *J. Atmos. Sci.*, **35,** 1125–1130.

——, and R. R. Garcia, 1979: A mechanistic model of ozone transport by planetary waves in the stratosphere. *J. Atmos. Sci.*, **36,** 350–364.

Holton, J. R., and W.-K. Choi, 1988: Transport circulation deduced from SAMS trace species data. *J. Atmos. Sci.*, **45,** 1929–1939.

Labitzke, K., 1972: The interaction between the stratosphere and mesosphere in winter. *J. Atmos. Sci.*, **29,** 1395–1399.

Lau, K.-M., and P. H. Chan, 1983: Short-term climate variability and atmospheric teleconnections from satellite-observed outgoing longwave radiation. Part II: Lagged correlations. *J. Atmos. Sci.*, **40,** 2751–2767.

Leovy, C. B., C.-R. Sun, M. Hitchman, E. E. Remsburg, J. M. Russell III, L. L. Gordley, J. C. Gille, and L. V. Lyjak, 1985: Transport of ozone in the middle stratosphere: Evidence for planetary wave breaking. *J. Atmos. Sci.*, **42,** 230–244.

Madden, R. A., 1975: Oscillations in the winter stratosphere: Part 2. The role of horizontal eddy heat transport and the interaction of transient and stationary planetary-scale waves. *Mon. Wea. Rev.*, **103,** 717–729.

——, 1983: The effect of the interference of traveling and stationary waves on time variations of the large-scale circulation. *J. Atmos. Sci.*, **40,** 1110–1125.

Perliski, L. M., and J. London, 1989: Satellite observed long-term averaged seasonal and spatial ozone variations in the stratosphere. *Planet. Space Sci.*, **37** (12), 1509–1525.

Plumb, R. A., 1982: Zonally symmetric Hough modes and meridional circulations in the middle atmosphere. *J. Atmos. Sci.*, **39,** 983–991.

Randel, W. J., 1993: Global normal mode Rossby waves observed in stratospheric ozone data. *J. Atmos. Sci.*, **50,** 406–420.

——, D. E. Stevens, and J. L. Stanford, 1987: A study of planetary waves in the southern winter troposphere and stratosphere. Part II: Life cycles. *J. Atmos. Sci.*, **44,** 936–949.

Rose, K., and G. Brasseur, 1989: A three-dimensional model of chemically active trace species in the middle atmosphere during disturbed winter conditions. *J. Geophys. Res.*, **94,** 16 387–16 403.

Schoeberl, M. R., and A. J. Krueger, 1983: Medium scale disturbances in total ozone during Southern Hemisphere summer. *Bull. Amer. Meteor. Soc.*, **64,** 1358–1365.

Shiotani, M., 1992: Annual, quasi-biennial, and El Niño–Southern Oscillation (ENSO) time-scale variations in equatorial total ozone. *J. Geophys. Res.*, **97,** 7625–7633.

Solomon, S., J. T. Kiehl, R. R. Garcia, and W. Grose, 1986: Tracer transport by the diabatic circulation deduced from satellite observations. *J. Atmos. Sci.*, **43,** 1603–1617.

Stanford, J. L., J. R. Ziemke, and S. Y. Gao, 1993: Stratospheric circulation features deduced from SAMS constituent data. *J. Atmos. Sci.*, **50,** 226–246.

Stolarski, R. S., and A. R. Douglass, 1985: Parameterization of the photochemistry of stratospheric ozone including catalytic loss processes. *J. Geophys. Res.*, **90,** 10 709–10 718.

——, P. Bloomfield, R. D. McPeters, and J. R. Herman, 1991: Total ozone trends from NIMBUS 7 TOMS data. *Geophys. Res. Lett.*, **18,** 1015–1018.

Sun, C.-R., and C. Leovy, 1990: Ozone variability in the equatorial middle atmosphere. *J. Geophys. Res.*, **95,** 13 829–13 849.

World Meteorological Organization (WMO), 1991: Report of the International Ozone Trends Panel—1988, WMO Rep. 18, World Meteorological Organization, Geneva, 829 pp.